Title	Origin of spurious single forces in the course mechanism of volcanic seismicity
Authors(s)	De Barros, Louis, Lokmer, Ivan, Bean, Christopher J.
Publication date	2013-07-15
Publication information	De Barros, Louis, Ivan Lokmer, and Christopher J. Bean. “Origin of Spurious Single Forces in the Course Mechanism of Volcanic Seismicity” 262, no. 15 July 2013 (July 15, 2013).
Publisher	Elsevier
Item record/more information	http://hdl.handle.net/10197/5682
Publisher's statement	This is the author’s version of a work that was accepted for publication in Journal of Volcanology and Geothermal Research. Changes resulting from the publishing process, such as peer review, editing, corrections, structural formatting, and other quality control mechanisms may not be reflected in this document. Changes may have been made to this work since it was submitted for publication. A definitive version was subsequently published in Journal of Volcanology and Geothermal Research (VOL 262, ISSUE 15 July 2013, (2013)) DOI: 10.1016/j.jvolgeores.2013.06.006
Publisher's version (DOI)	10.1016/j.jvolgeores.2013.06.006

Origin of spurious single forces in the source mechanism of volcanic seismicity.

Louis De Barros[a,b,*], Ivan Lokmer[a,*], Christopher J. Bean[a,*]

[a] *School of Geological Sciences, University College Dublin, Dublin, Ireland.*
[b] *Now at: Geoazur, Université Nice-Sophia Antipolis, CNRS, Observatoire de la Côte d'Azur, Sophia-Antipolis, France*

Abstract

Single forces are often observed in the source mechanism of volcanic seismicity. However, their underlying causative processes are still doubtful. The reliability of single force observations must be assessed, prior to analysing them in terms of physical mechanisms. Using numerical examples, we show that source mislocation and velocity mismodeling lead to strong spurious single forces. Layering in the velocity model produces converted S-waves and source mislocations modify the wavefield at the free surface (mainly through converted S- and surface waves). However, these waves can also be accurately reproduced in a homogeneous model by adding a vertical single force in the source mechanism, which mainly generates S-waves for large take-off angles. Hence approximate velocity models can lead to the appearance of strong single forces in source inversions. We conclude that, in moment tensor inversion, while single forces can be used in some cases to accommodate mismodeling errors, they cannot be reliably used to infer physical processes.

Keywords: Volcano seismicity, Source mechanism, Single forces

---

[*] Corresponding author
Email address: `louis.debarros@unice.fr` (Louis De Barros)

---

1. Introduction

Moment Tensor Inversion (MTI) is an extensively used tool to characterize the source mechanism of seismic events. When applied to volcanic seismicity, such as Long Period events (LP, with a main period of 1s here) (e.g. Kumagai et al., 2002; Lokmer et al., 2007; De Barros et al., 2011), Very Long Period events (VLP, with a main period of 20s here) (e.g. Ohminato et al., 1998; Chouet et al., 2003) and tremors (Davi et al., 2012), the resulting mechanisms usually exhibit a strong volumetric component (see Chouet and Matoza, 2013, and references therein). In earthquake seismology, MTI is usually limited to the reconstruction of the 6 components of the Moment Tensor (MT) of the equivalent point source, but in volcanic applications the 3 components of Single Forces (SF) are usually added (Ohminato et al., 1998). The recovered SFs often have strong amplitude (e.g. Ohminato et al., 2006; De Barros et al., 2011).

As shown by theoretical considerations (e.g., Takei and Kumazawa, 1994) or by laboratory experiments (e.g., James et al., 2004), SFs can be generated by mass transfer or by viscous fluid movement in the volcano. They are usually interpreted in terms of magma upwelling in conduits when observed in volcanic seismicity (Chouet et al., 2003; Ohminato et al., 2006). SFs have therefore been used to strongly constrain the source processes of the volcanic seismicity. However, as shown firstly by Ohminato et al. (1998) and Chouet et al. (2003), and later by Bean et al. (2008) and De Barros et al. (2011), uncertainties in both source location and velocity structure can lead to the reconstruction of strong spurious SFs.

LP and VLP events are found to be shallow, in the first kilometer below the surface (see e.g. Chouet et al., 2003; De Barros et al., 2009; Inza et al., 2011). The upper part of the volcanic edifice is made of compliant and weathered materials, leading to low and highly heterogeneous seismic velocities (e.g., Chouet et al., 1998; Mora et al., 2006; Cauchie and Saccorotti, 2013). However, the detailed velocity structure is usually poorly known, hence homogeneous velocity models are commonly used when calculating Green's Functions (GFs) in MTI. This simplification is generally justified by the use of long wavelengths (especially for VLP), which are similar to the propagation distances. However, the lack of knowledge of the velocity structure leads to uncertainties in source location (particularly for the depth parameter) for joint location and MT inversion (Lokmer et al., 2007) or location only (De Barros et al., 2009). It is now well documented that MTI can suffer from a badly constrained velocity model (Jousset et al., 2004; Bean et al., 2008; Kumagai et al., 2011), especially for the highest frequency (LP). However, for both LP and VLP cases, it is not clear yet if SF should be included or not in the inversion, and if they can be unequivocally interpreted as physically present.

The aim of this paper is to numerically investigate why errors in the velocity model and in the source locations generate apparent source related SFs, and as a consequence, if it is meaningful to infer a physical process from SFs. We will first show on synthetic data computed in models of Mt Etna (De

Barros et al., 2011) the effect on SFs of slight velocity modeling and sources location errors. We then simplify the problem in order to be able to identify the different waves responsible for the SF reconstruction, and generalize our findings to all frequency ranges.

2. Single forces in synthetic tests

Bean et al. (2008) showed that mismodeled complex media can have a detrimental effect on MT solutions for shallow volcanic sources. They suggest using stations as close as possible to the source. For this reason, a high-resolution experiment was undertaken on Mt Etna in 2008, including 30 stations within 2 km of the source area. De Barros et al. (2011) performed a MTI of the LP events recorded by this network. Here, using the same set-up, we compute synthetic data and GFs using the full wavefield elastic lattice algorithm of O'Brien and Bean (2004), including the topography of Mt Etna with a 40 m grid step. The GFs are calculated for a homogeneous model (Vp_0=2000 m/s,Vs_0=$Vp_0/\sqrt(3)$, ρ=2300 kg/m^3), for a 400 m deep source. Synthetic data are computed for two cases: 1) velocity mismodeling case: a 200 m layer (Vp=1600 m/s) following real Mt Etna topography over a half-space with a 2400 m/s velocity; and 2) mislocation case: the homogeneous velocity model is used and the source location is misplaced by 120 m downward and by 90 m horizontally. The source has a 1 Hz Ricker wavelet time function and a vertical crack ([3,1,1] $\times 5\ 10^{12}$ Nm) mechanism.

The MTI is performed in the frequency domain, with a fixed source location. In both cases (see fig. 1), and because of the exceptional number of stations in the close proximity of the source, the source time function (STF) and the mechanism of the MT are quite well reconstructed, unlike the amplitudes. The amplitudes are in fact inversely proportional to the velocity (eq. 4.29, Aki and Richards, 2002). A slight time shift exists between the STFs of the different MT components, but the decomposition leads to a near perfect [3,1,1] solution in both cases. The accuracy of the MT solution is ensured here by the exceptionally dense network (De Barros et al., 2011). However, strong SFs appear, with amplitudes reaching more than 5.5 10^9 N. SFs are mainly in the vertical direction for the velocity mismodeling case, and are inclined for the source mislocation case. Note that an amplitude of 10^9 N from the SF source and of 10^{12} Nm for a MT source lead to seismic waves of the same order of magnitude when the radiation pattern is neglected (see eq. 4.27 and 4.28 in Aki and Richards (2002)). Hence, even in such a simple case, both location and velocity mismodelings give rise to strong spurious SFs.

3. Origin of single forces

To understand the relationship between the mismodeling and the spurious SFs, we simplify the problem even further: we calculate synthetic waveforms generated by a purely isotropic source (1 Hz Ricker wavelet signature) in a medium without topography. In this way, the source generates only a P-wave, and all complex signatures can be attributed to the propagation effects. The different waves can be easily identified, allowing us to determine which waves are responsible for the spurious SF generation. The synthetic data are computed using the SKB code (Dietrich, 1988) based on the reflectivity method of Kennett (1983), coupled with the wavenumber integration of Bouchon and Aki (1977).

Following the results from the previous section, we assume that the mechanism and the STF of the MT components are properly recovered, but not the amplitude. We therefore constrain the inversion to a fixed mechanism (explosion) and STF (1 Hz Ricker wavelet), and invert for the amplitudes of the explosion and of the SFs required to accommodate the modeling uncertainties. Hence, by constraining the mechanism, we focus exclusively on the SFs reconstruction due to the modeling errors.

Synthetic data $\boldsymbol{U_{Ex}^{True}}$ are calculated from an explosion in two models ("true" models, see tab. 1): 1) a 2-layer model M^1_{True} to investigate velocity mismodeling effects, and 2) a homogeneous model M^2_{True}, with a shallow-source location, to investigate mislocation effects. We also calculate a set of signals in an homogeneous model (hereinafter referred as "approximate" model M_{app}, see tab. 1). This approximate model is equivalent to the model used in MTI in which Green's functions are computed. Similarly to MTI of volcano data, this model is assumed to be the best model (usually homogeneous) we have to represent the complex structure of the volcano. The signals are generated by an explosion ($\boldsymbol{U_{Ex}^{app}}$) and SFs ($\boldsymbol{U_{F}^{app}}$). In all models, the amplitude of the isotropic source is 10^{12} Nm, and the amplitude of the SFs in the M_{app} model is 10^9 N.

The data computed in the approximate model ($\boldsymbol{U_{Ex}^{app}}$ and $\boldsymbol{U_{F}^{app}}$) are used to reconstruct the synthetic signals ($\boldsymbol{U_{Ex}^{True}}$) computed in the "true" models, such as:

$$\boldsymbol{U_{Ex}^{True}} = \alpha_{Ex}\, \boldsymbol{U_{Ex}^{app}} \ + \ \alpha_F\, \boldsymbol{U_F^{app}} \tag{1}$$

α_{Ex} and α_F are the amplitudes of the explosion and of the SFs in the "approximate" model, respectively, needed to fit the the synthetic data (isotropic source in the M_{True} model). Since the sources have the same magnitude in the both true and approximate models, the amplitudes α_{Ex} and α_F can be seen as normalised amplitudes or magnitude correction factors. In order to reconstruct the synthetic data, these parameters are inverted to minimize the least square difference between the two sides of this equations. This inversion is performed in the frequency domain. Since the velocity models are different, time shifts might exist between the data, which are corrected by inverting for complex coefficients α_{Ex} and α_F. However, only the real part of these coefficients is later considered as the reconstructed imaginary part is negligible (more than 17 orders of magnitude smaller than the real part). In this inversion, either an explosion only (Ex), or an explosion and a vertical SF (Ex&Fz) or an explosion and two SFs (Ex&F) were considered. Hence, this is equivalent to a MTI where the MT part is constrained to an explosion with a known STF, and with or without SFs. We also define a misfit function in the least square sense as:

$$MIS = \frac{\sum_{t_i}^{L} \left[\boldsymbol{U_{Ex}^{True}}(t_i) - (\alpha_{Ex} \ \ \boldsymbol{U_{Ex}^{app}}(t_i) \ + \ \alpha_F \ \ \boldsymbol{U_F^{app}}(t_i))\right]^2}{\sum_{t_i}^{L} \left[\boldsymbol{U_{Ex}^{True}}(t_i)\right]^2} \tag{2}$$

3.1. Velocity mismodeling

The synthetic data are computed in the 2-layer model (M_{True}^1, see table 1). To isolate the effects of the interface, the free surface is "switched off", leading to two joined half-spaces. The top layer (Vp_1=1600 m/s) contains a line of receivers 200 m above the interface. The explosion, in the second layer (Vp_2=2400 m/s), is located 200 m below the interface between the two layers. The simulation in the medium M_{app} is carried out with the same geometry, but with a homogeneous velocity of 2000 m/s.

The synthetic data (vertical component) are shown in figure 2a. Even though the explosive source only produces P-waves, the wavefield above the interface contains S-waves, generated by the P-to-S conversion at the interface, with amplitudes stronger than the transmitted P-waves. In the model M_{app}, the explosive source produces only P-waves, whilst a vertical force at such large take-off angles mainly generates S-waves (fig. 2b). The waveforms in fig. 2a looks very similar to the sum of the waveforms in fig 2b. Qualitatively, it seems that, to reconstruct the seismic waveforms generated in the two-layer medium, SFs are needed in the homogeneous medium in order to fit the high energy converted waves. Using the inversion process previously described, the misfit decreases from 51 % when an explosion only (Ex) is considered in eq. (1) to 12 % (α_F=4.2 and α_{Ex}=1) when a vertical SF is included (Ex&Fz) in the inversion. Since they are no single forces in the original data for the two layered medium, these large SFs are spurious.

We investigate the variations in amplitude of the apparent SFs as a function of the contrast between the two layers, by changing the velocity Vp_1 in the top layer. The misfit between the reconstructed and synthetic data is given in fig. 2c, and fig. 2d shows the normalised amplitude of the explosion

α_{Ex} and SFs α_F required in the approximate model. As expected, when there is no contrast, no SFs are found. When $Vp_1 > Vp_2$, although significant SFs can be found, the misfit does not change much whether or not SF are included. In contrast, the amplitude of the SF strongly increases when $Vp_1 < Vp_2$ (i.e. low velocity layer on top of the volcano), leading to a misfit value roughly constant for Vp_1 between 1400 and 2600 m/s. When Vp_1 is even lower, strong SF are still found, but the waveform reconstruction deteriorates. These simple examples show that the presence of a mismodeled low velocity layer on the top of the volcano will lead to strong SF in the mechanism reconstruction with a high misfit difference between inversion with and without SF. As the layers in a volcano are certainly not horizontal, strong horizontal SFs might also be reconstructed to accommodate converted waves.

The similarity of the response between the amplitude of the P-to-S converted waves and the Fz radiation pattern can be illustrated by comparing the theoretical AVA (Amplitude Versus Angle) response of i) an explosion in the two-layer medium M^1_{True}, and ii) of a vertical SF and an explosion in the homogeneous medium M_{app}, for both P and S waves (fig. 2e). This brings into play the radiation patterns of the source, the transmission coefficients and the geometrical spreading, as defined in Aki and Richards (2002). The angle is defined as the $\arctan(Xs/Zs)$, where Xs and Zs are the horizontal and vertical offset from the source, respectively. It corresponds to the incidence angle only in the homogenous case. In the medium M_{app}, P-waves are coming from both the SF and the explosion, and S-wave are generated by the SF only. Both P transmitted and S converted waves generated by the explosion in the 2-layer medium have amplitudes that can be fitted remarkably well with an explosion and a SF in the homogeneous medium, especially for angles less than 50^o. The amplitudes of the waves in the "true" and in the "approximate" medium are still very similar for higher angles.

3.2. Source mislocation

A similar analysis is performed to evaluate why SFs appear in MTI when the source is mislocated (fig. 1b). Synthetic data are computed in the homogeneous model M^2_{True} with a free surface and a source located at 200 m depth (tab. 1). This model is approximated by the model M_{app}, with the source at 400 m depth, i.e. vertically mislocated by 200 m. Figure 3a shows the dataset calculated from an explosive source in both media. While P-waves look very similar, surface waves and S-converted waves at the surface strongly differ in amplitude. When a vertical SF is included in the model M_{app} (fig. 3b), the waveform fit is far better, with a misfit decreasing from 37% (Ex only) to 16% (Ex&Fz). The SF amplitude is once again very strong, with $\alpha_{Ex} = 1.1$ and $\alpha_F = 2.9$.

We then modify the source depth Z_{true} from 0 to 800 m in the model M^2_{True} (see Fig. 3c and d), while the source location in the M_{app} model is kept at 400 m depth. When the source in M_{app} is shallower than Z_{true} (i.e $Z_{true} > 400$ m), SFs are not reconstructed. On the other hand, for shallow sources mismodeled by deeper ones (i.e $Z_{true} < 400$ m), the amplitudes of the SF increase with the depth errors and the misfit difference between Ex only and Ex&F reconstructions is quite strong. Hence, vertical SFs are found when the source depth is over estimated. In the presence of topography, horizontal SFs may also be required to compensate for an imperfect source location, as shown in fig. 1.

3.3. Other frequency range

In order to generalise our findings to a broader frequency range, we carry out the same two tests as described in Sect. 3.1 and 3.2, for a suite of source-time functions (Ricker wavelets) with the central frequency ranging from 0.05 to 2 Hz. The results are given in Figure 4. For the VLP wavelet (F_{peak}=0.05 Hz) without the inclusion of SFs, velocity mismodeling and mislocation result in a small misfit between the synthetic and reconstructed data (0.25% and 4%, respectively, Figs. 4a and c). This is because the travel time differences caused by different velocity models and/or locations are negligible compared to the dominant period of STF. When a vertical SF is included, the misfits decrease to 0.07% and 2.2%, respectively, that is, by a factor of 2-5. Although the absolute values of these decreases are small, spurious SFs of relatively large amplitudes are reconstructed, with α_F=0.3 and α_F=-1.5 for the mismodeling and mislocation case, respectively (Figs. 4b and d) .

Such a result is in agreement with Ohminato et al. (1998) and Chouet et al. (2003) for the mislocation case, even if they consider much smaller source location errors or deeper source. For the velocity mismodeling case, they both used homogeneous models with different velocities to compute Green's functions and synthetic data. They found that no or very small spurious SFs are reconstructed. We agree with these authors that VLP inversion are not sensitive to a wrong homogeneous velocity. However, we showed here that spurious SFs are generated to accommodate converted waves at layer interfaces, which were not present in their tests. Our approach suggests that, at all frequencies, both velocity mismodeling and source mislocation can result in strong spurious SFs, which can heavily contaminate the real single forces, if they exist.

4. Discussion and conclusion

Using simple numerical examples, we showed that strong SFs are required to compensate for velocity mismodeling and source mislocation, for both LP and VLP signals. These examples are obviously too simple to reproduce the complexity of the seismic wavefield recorded in a volcanic environment, but they do capture the essence of the problems we face in terms of poor source locations and poorly constrained very near-surface velocity structure. They illustrate how spurious SFs are required in order to reconstruct the observed converted and surface waves, produced by an interface or the free surface.

As the sources of the non-shearing volcanic seismicity are usually very shallow, take-off angles are large. Hence, a vertical SF mainly generates S-waves at the recording stations. If the medium is approximated with a smooth or homogeneous medium, converted P-to-S waves at any interfaces are not modeled and are accommodated by apparent SFs in the source. In particular, low velocity layers have been commonly observed on the top of the volcano, for examples on Mt Etna (Cauchie and Saccorotti, 2013), Vesuvius (Saccorotti et al., 2001) and Arenal (Mora et al., 2006). They are usually not considered in MTI. A location error of a few hundred meters is more the rule than the exception in volcanic environments, and can lead to spurious SFs, to accommodate converted S-waves and surface waves. In both cases, the spurious SFs produce waves with comparable amplitudes as those from the MT part of the solution.

Since shallow layers are usually not known, it may be useful to use SFs in MTI to accommodate errors arising from unmodeled layers (De Barros et al., 2011). However, such an approach requires a high-resolution seismic network, otherwise the MT solution might not be correctly reconstructed (Bean et al., 2008). In cases where SFs are actually real, they will be corrupted by strong spurious SFs which inevitably exist as demonstrated herein. Their physical processes cannot be unambiguously interpreted. On the other hand, the presence of strong SFs may give an indication of the presence of a layered structure and the best source location may be where the inversion misfits with and without forces are similar.

The misfit difference between MTI with and without SFs may be quite large and comes from the mismodeling and not from inversion for the sources itself. Hence, the misfit cannot be used directly or through Akaike or BIC criteria to determine if SFs should be used in the inversion (O'Brien et al., 2010). We recommend that synthetic tests as outlined above with mismodeling are undertaken in order to decide whether SFs should be included or not. As the source locations are shallow, stations above the source area are required to stabilize the inversion and achieve lower amplitude spurious SFs. Furthermore, as already noted by Bean et al. (2008), improving the source mechanism reconstruction will firstly require improvements in velocity models, especially in the shallow parts of the edifice.

5. Acknowledgments

L. De B. was part funded by the department of Communications, Energy and Natural Resources (Ireland) under the National Geosciences programme 2007-2013. Computational facilities from SFI/HEA ICHEC are acknowledged. We thank Michel Dietrich (ISTerre, Grenoble, France) for the SKB code.

6. Bibliography

Aki, K., Richards, P., 2002. Quantitative seismology. University Science Books, Sausalito, Calif.

Bean, C., Lokmer, I., O'Brien, G., 2008. Influence of near-surface volcanic structure on long-period seismic signals and on moment tensor inversions: Simulated examples from Mount Etna. J. Geophys. Res. 113. doi:10.1029/2007JB005468.

Bouchon, M., Aki, K., 1977. Discrete wave-number representation of seismic-source wave fields. Bull. Seism. Soc. Am. 67, 259–277.

Cauchie, L., Saccorotti, G., 2013. Probabilistic inversion of Rayleigh-wave dispersion data: an application to Mt.Etna, Italy. J. Seismol. 17, 335–346.

Chouet, B., Dawson, P., Ohminato, T., Martini, M., Saccorotti, G., Giudicepietro, F., De Luca, G., Milana, G., Scarpa, R., 2003. Source mechanisms of explosions at Stromboli Volcano, Italy, determined from moment-tensor inversions of very-long-period data. J. Geophys. Res. 108, 2019–2042. doi:10.1029/2002JB001919.

Chouet, B., De Luca, G., Milana, G., Dawson, P., Martini, M., Scarpa, R., 1998. Shallow velocity structure of Stromboli volcano, Italy, derived from small-aperture array measurements of Strombolian tremor. Bull. Seism. Soc. Am. 88, 653–666.

Chouet, B.A., Matoza, R.S., 2013. A multi-decadal view of seismic methods for detecting precursors of magma movement and eruption. J. Volcanol. Geotherm. Res. 252, 108–175.

Davi, R., O'Brien, G.S., De Barros, L., Lokmer, I., Bean, C.J., Lesage, P., Mora, M.M., Soto, G.J., 2012. Seismic source mechanisms of tremor recorded on Arenal volcano, Costa Rica, retrieved by waveform inversion. J. Volcanol. Geotherm. Res. 213-214, 1–13.

De Barros, L., Bean, C., Lokmer, I., Saccorotti, G., Zuccarello, L., O'Brien, G., Métaxian, J.P., Patanè, D., 2009. Source geometry from exceptionally high resolution long period event observations at Mt Etna during the 2008 eruption. Geophys. Res. Lett. 36. doi:10.1029/2009GL041273.

De Barros, L., Lokmer, I., Bean, C., O'Brien, G., Saccorotti, G., Métaxian, J.P., Patanè, D., Zuccarello, L., 2011. Source characteristics of Long Period event at Mt Etna during the 2008 eruption. J. Geophys. Res. 116, B01304. doi:10.1029/2010JB007629.

Dietrich, M., 1988. Modeling of marine seismic profiles in the t-x and tau-p domains. Geophysics 53, 453–465.

Inza, L.A., Mars, J.I., Métaxian, J.P., O'Brien, G.S., Macedo, O., 2011. Seismo-volcano source localization with triaxial broad-band seismic array. Geophy. J. Int. 187, 371–384.

James, M., Lane, S., Chouet, B., Gilbert, J., 2004. Pressure changes associated with the ascent and bursting of gas slugs in liquid-filled vertical and inclined conduits. J. Volcanol. Geotherm. Res. 129, 61–82.

Jousset, P., Neuberg, J., Jolly, A., 2004. Modelling low-frequency earthquakes in a viscoelastic medium with topography. Geophy. J. Int. 159, 776–802.

Kennett, B., 1983. Seismic Wave Propagation in Stratified Media. 342 p, Cambridge University Press, Cambridge.

Kumagai, H., Chouet, B., Nakano, M., 2002. Waveform inversion of oscillatory signatures in long-period events beneath volcanoes. J. Geophys. Res. 107, 2301–2312.

Kumagai, H., Saito, T., O'Brien, G., Yamashina, T., 2011. Characterization of scattered seismic wavefields simulated in heterogeneous media with topography. J. Geophys. Res. 116, B03308.

Lokmer, I., Bean, C.J., Saccorotti, G., Patanè, D., 2007. Moment-tensor inversion of LP events recorded on Etna in 2004 using constraints obtained from wave simulation tests. Geophys. Res. Lett. 34. doi:10.1029/2007GL031902.

Mora, M., Lesage, P., Valette, B., Alvarado, G., Leandro, C., Métaxian, J.P., Dorel, J., 2006. Shallow velocity structure and seismic site effects at Arenal volcano, Costa Rica. J. Volcanol. Geotherm. Res. 152, 121–139.

O'Brien, G., Bean, C., 2004. A 3D discrete numerical elastic lattice method for seismic wave propagation in heterogeneous media with topography. Geophys. Res. Lett. 31. doi:10.1029/2004GL020069.

O'Brien, G.S., Lokmer, I., Bean, C.J., 2010. Statistical selection of the "best" seismic source mechanisms from inversions of synthetic volcanic long-period events. J. Geophys. Res. 115, B09303. doi:10.1029/2009JB006958.

Ohminato, T., Chouet, B.A., Dawson, P., Kedar, S., 1998. Waveform inversion of very long period impulsive signals associated with magmatic injection beneath Kilauea Volcano, Hawaii. J. Geophys. Res. 103. doi:10.1029/98JB01122.

Ohminato, T., Takeo, M., Kumagai, H., Yamashina, T., Oikawa, J., Koyama, E., Tsuji, H., Urabe, T., 2006. Vulcanian eruptions with dominant single force components observed during the Asama 2004 volcanic activity in Japan. Earth, Planets, and Space 58, 583–593.

Saccorotti, G., Maresca, R., Del Pezzo, E., 2001. Array analyses of seismic noise at Mt. Vesuvius volcano, Italy. J. Volcanol. Geotherm. Res. 110, 79–100.

Takei, Y., Kumazawa, M., 1994. Why have the single force and torque been excluded from seismic source models? Geophy. J. Int. 118, 20–30.

	SRC	Zsrc (m)	Vp (m/s)
M^1_{True}	Ex	400	1600/2400
M^2_{True}	Ex	200	2000
M_{app}	Ex/Ex&Fz	400	2000

Table 1: Velocity models used in this study. M^1_{True} (layered model) and M^2_{True} (shallow source model) are the "true" models, and M_{app} is the "approximate" model (equivalent to the medium where the GFs are computed in a MTI). The data computed in the true models with an explosive source are reconstructed using data generated in the model M_{app} by i) an explosion only (Ex) or ii) by an explosion and SF (Ex&F). Zsrc denotes the source depth, while V_P is the P-wave velocity used in the calculation. The 12 receivers are at Z=0, with horizontal offsets ranging from 250m to 3000m from the source.

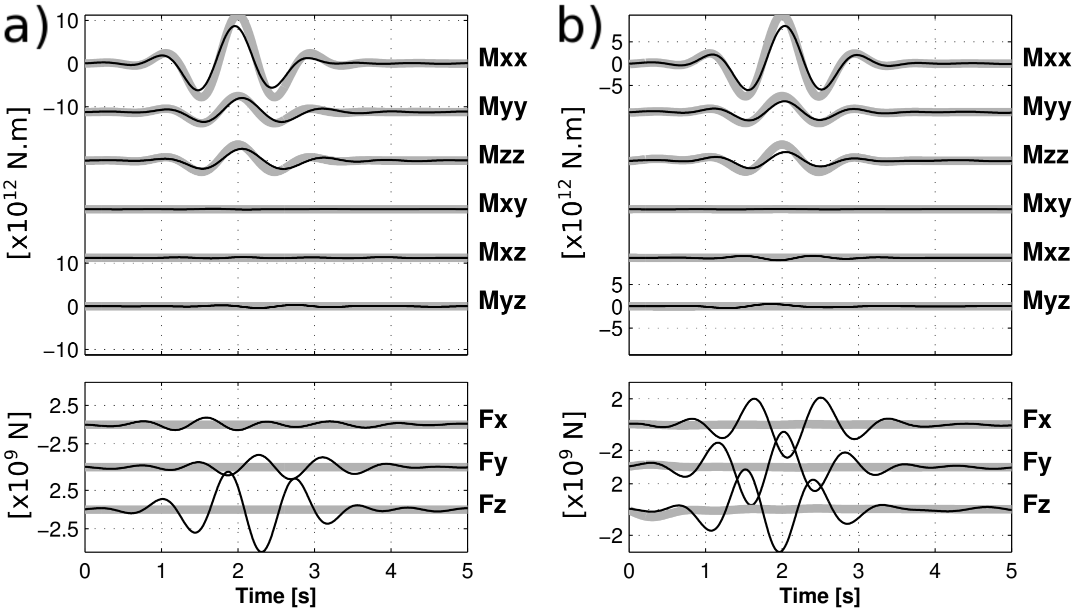

Figure 1: Solutions of the Moment Tensor Inversion of synthetic data computed for a vertical crack source (Mxx=3*Myy=3*Mzz) in the Mt Etna geometry. a) Data computed in a layered medium and inverted with GFs calculated in a homogeneous medium; b) Data computed in homogeneous medium and inverted with GFs calculated for a source mislocated by 120 m downward and 90 m horizontally. For both cases, gray thick lines are the true solutions and the black lines are the reconstructed solution for the 6 moment components and the 3 SFs.

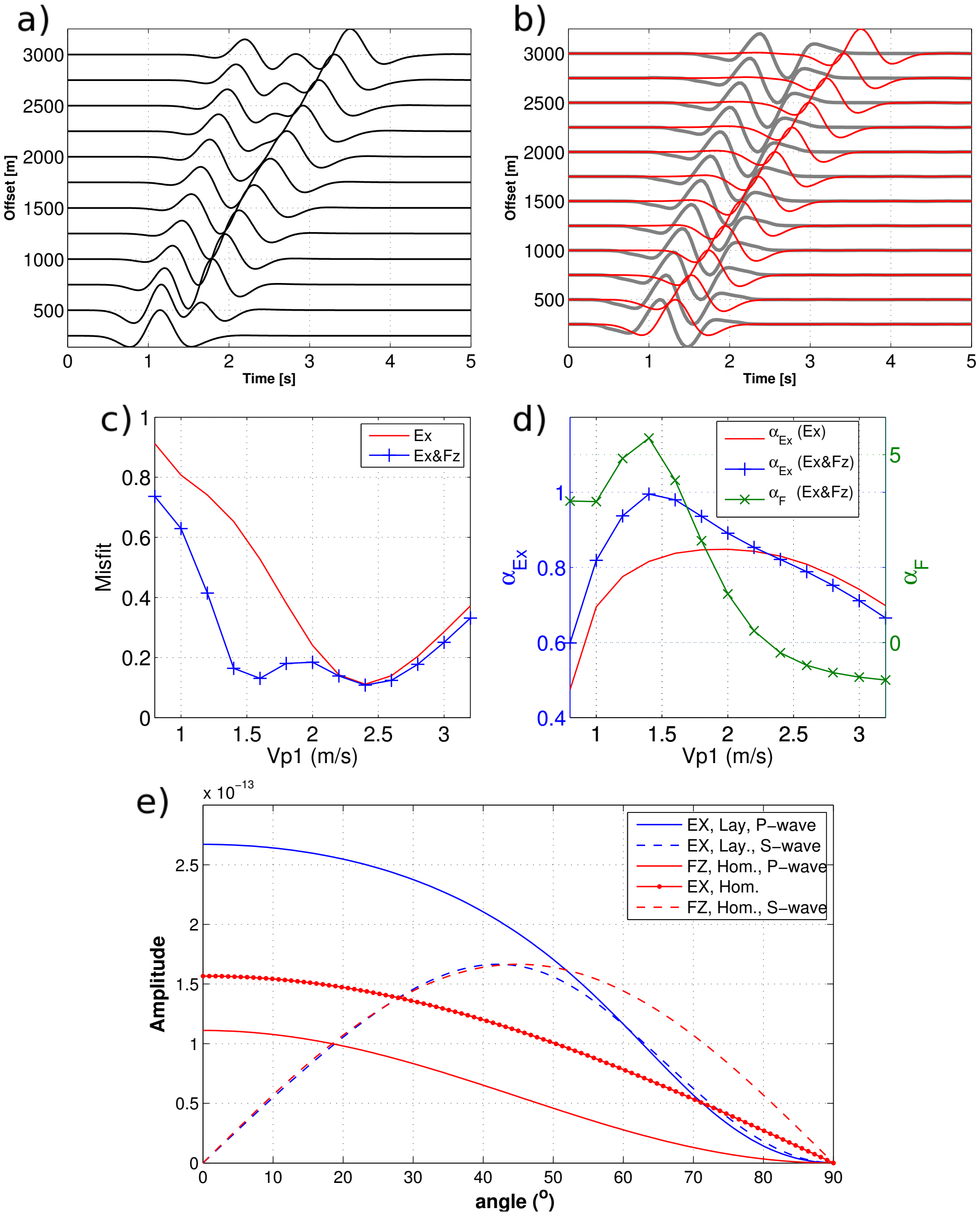

Figure 2: Apparent SFs generated by a velocity model error. a) Synthetic “True” data computed in the two-layer model (M^1_{True}, with Vp_1=1600 m/s and Vp_2=2400 m/s), with an explosion located 200 m below the interface. No free surface is included. Receivers are 200 m above the interface. b) Waveforms computed in the medium M_{app} for an explosion (thick line) and a vertical SF (thin red line). Note that each trace is normalized in a) and b). c) Misfits in the reconstruction using an explosion only (Ex) and an explosion and a vertical force (Ex&Fz), as a function of the velocity Vp_1 in the model M^1_{True}. d) Amplitude of the explosion (left scale, α_{Ex}) and the SF Fz (right scale, α_F) for the Ex only and the Ex&Fz reconstruction. e) Theoretical Amplitude Versus Angle (AVA) response for an explosion and a vertical SF in the homogeneous medium M_{app}, and transmitted P- and S- waves generated by an explosive source in the 2-layer medium M^1_{True}.

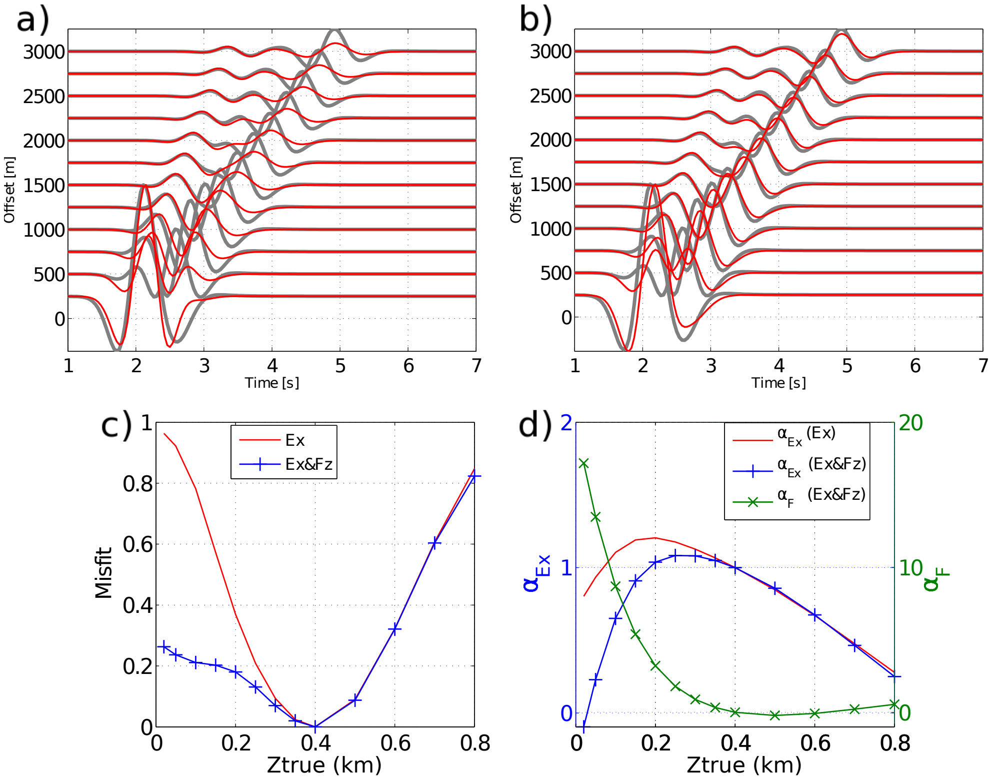

Figure 3: Apparent SFs generated by an incorrect source location. a) Synthetic data computed in the "true" model (M^2_{True}) with an explosive source located at Z_{true}=200 m (thick lines) and in the "approximate" medium M_{app} with an 400m-deep explosive source (Ex) (thin red lines). b) Same as a) with explosive and vertical SF (Ex&Fz) sources in the model M_{app}. c) Misfit between the two data-sets using Ex only or Ex&Fz in the model M_{app}, as a function of the depth Z_{true} of the source in the "true" model. d) Amplitude of the explosion (α_{Ex}, left scale) and the force Fz (α_F, rigth scale) for the reconstruction using an explosion only (Ex) only and an explosion and vertical force (Ex&Fz).

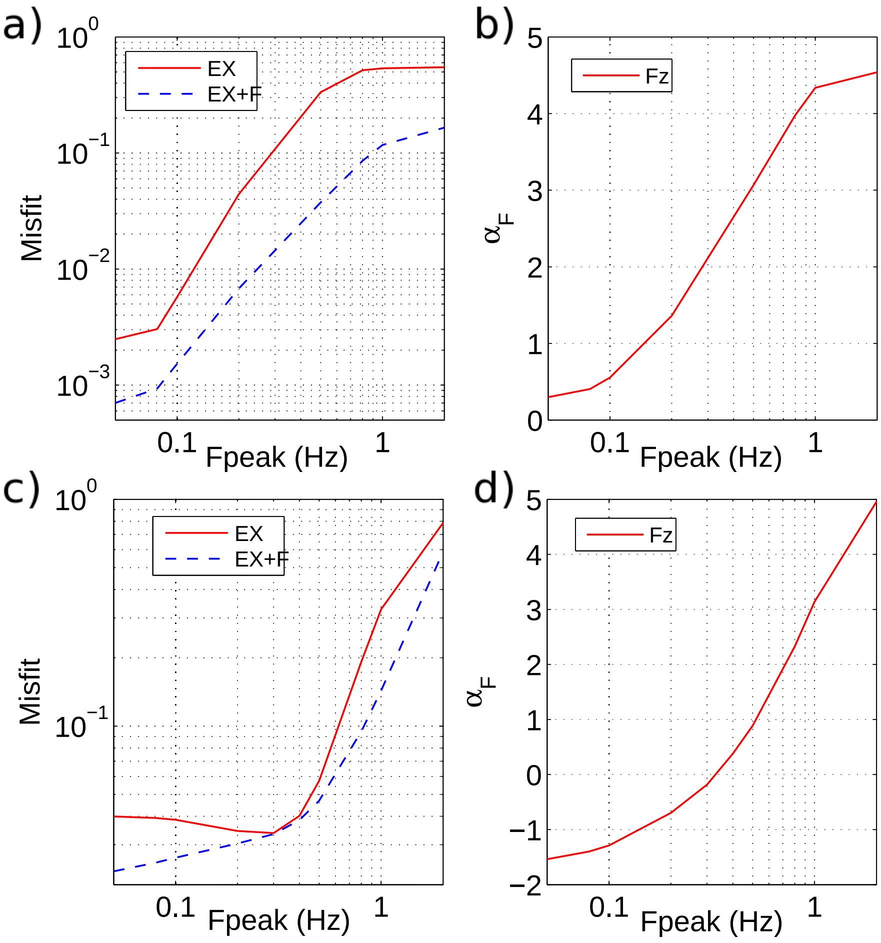

Figure 4: Generation of spurious SFs as a function of the peak frequency $Fpeak$ of the source time function (Ricker wavelet). Velocity mismodeling case (same set-up as for fig. 2): a) misfit between the synthetic data and the reconstructed waveforms using an explosion only (Ex, solid line) and an explosion and a vertical SF (Ex+SF, dashed line), b) the amplitude α_F of the vertical SF. c) and d) are the same as a) and b) but for the source mislocation case (same set-up as for fig. 3). Note that the spurious SF changes sign with the increasing frequency, and is therefore null for $Fpeak$=0.35 Hz.